The 15th International Symposium on Magnetic Bearings, August 3-6, 2016, Mojiko Hotel, Kitakyushu, Japan

ISMB15

Laboratory Tests on an interconnected four poles magnetic bearing

D. F. B. DAVID*, J. A. SANTISTEBAN* and A. C. DEL NERO GOMES**

* Universidade Federal Fluminense
Rua Passo da Ptria 156, 20420-240 Niteroi, Brasil
** COPPE — Engenharia Eltrica
Universidade Federal do Rio de Janeiro, Rio de Janeiro, Brasil
E-mail: nero@coep.ufrj.br

Abstract

A new structure for active magnetic bearings, based on a successfull idea used in self-bearing motors, has been recently discussed in the literature. A flux interconnection characterizes this idea, and theoretical results predict some advantages of this new model, when compared with the traditional one, with independent flux paths. As an example, a greater equivalent stiffness is expected for this new type of bearing. Two recently built prototypes were used to check whether these expectations really hold true. The main goal of this paper is to present and discuss the prototype details.

Key words : Active magnetic nearings, Reluctance forces, Control of magnetic bearings, Stiffness of magnetic bearings, interconnected flux magnetic bearings)

1. Introduction

The conventional active magnetic bearing, or AMB for short, can be studied in (Schweitzer et al., 1994) (Chiba et al., 2005) (Schweitzer et al., 2009). This traditional AMB, here called Type A, is based on the structure shown in Fig. 1: there are four “U-shaped electromagnets”, two for acting in the x direction and two in the y direction, resulting in four independent magnetic flux loops.

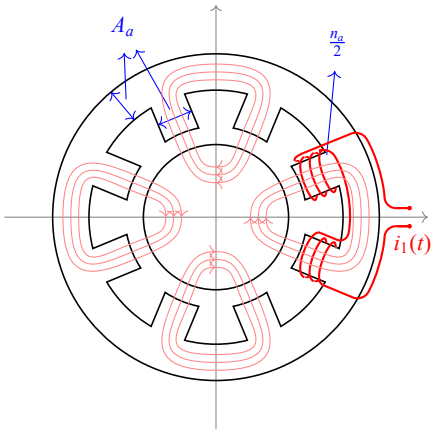

Fig. 1 Type A, or traditional, configuration for AMBs; windings are shown for the positive x direction only; there are no connections among the flux paths. Opposing pairs of windings along the x (y) direction control the horizontal (vertical) position.

The windings in the x and y directions are fed with currents $i_0 \pm i_x(t)$ and $i_0 \pm i_y(t)$, where the constant i_0 is the base, or bias, current, and the differential currents i_x and i_y control the rotor position. Using reluctance concepts, the resultant forces f_x and f_y can be expressed in terms of these currents, the air magnetic permeability μ_0, the number of coils n_a, the cross section area in the ferromagnetic material A_a and the nominal length h of the air gaps. After a linearization procedure (Schweitzer et al., 1994) around the operating point $x = y = i_x = i_y = 0$, the type A forces are shown in (1).

Notice that the non connected nature of the magnetic fluxes leads to uncoupled forces.

$$\left.\begin{array}{l} f_x = k_p^a x + k_i^a i_x \\ f_y = k_p^a y + k_i^a i_y \end{array}\right\} \quad \text{where} \quad \left\{\begin{array}{l} k_p^a = \mu_0 A_a n_a^2 i_0^2 / h^3 \\ k_i^a = \mu_0 A_a n_a^2 i_0 / h^2 \end{array}\right. \tag{1}$$

A different structure for magnetic bearings, here named Type B, is possible, with four windings that lead to interconnected magnetic loops, as depicted in Fig. 2. This structure is found in the self-bearing motors researched in Brazil (David, 2000) (Rodriguez and Santisteban, 2011), where alternate currents are injected in the windings to provide a simultaneous torque; for AMBs, DC currents are considered.

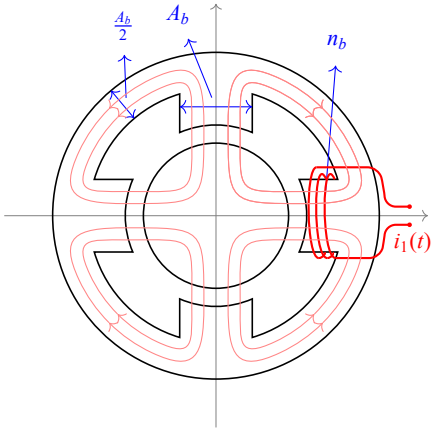

Fig. 2 Type B, the proposed configuration for AMBs; windings are shown for the positive x direction only; the flux paths are interconnected. Opposing pairs of windings along the x (y) direction control the horizontal (vertical) position.

The reluctance forces f_x and f_y in Type B were studied in (David et al., 2013) and (David et al., 2014); note that there are some typos affecting the flux indices in this last paper, but the main results hold true. After an algebraic procedure and a linearization stage, the following expressions were found

$$\left.\begin{array}{l} f_x = k_p^b x + k_i^b i_x \\ f_y = k_p^b y + k_i^b i_y \end{array}\right\} \quad \text{where} \quad \left\{\begin{array}{l} k_p^b = 2\mu_0 A_b n_b^2 i_0^2 / h^3 \\ k_i^b = 2\mu_0 A_b n_b^2 i_0 / h^2 \end{array}\right. \tag{2}$$

Two remarkable aspects are to be noted: (a) the fluxes are interconnected in type B, but the forces are decoupled, exactly as in type A; (b) a factor 2 appears in the formulas above, meaning that the position and current constants, k_p^b and k_i^b have higher values than in the A case. Although other results are known with the Type B bearing concept (Santos and Kjolhed, 2007), the authors of this article did not identify, up to the present time, the association of itsinterconnected structure with uncoupled equations for radial restoring forces or with higher values of the magnetic constants.

Section 2 presents analytical results and simulations on how increasing $k_{p,i}^b$ affects dynamic and control aspects of AMBs (David et al., 2014). Details of the protoypes built to allow real comparisons between types A and B are shown in section 3, while section 4 brings the simulations results. Discussions about real tests, final comments and considerations on what remains to be done are made in section 5.

2. Theoretical Comparisons

Assuming the same outside stator diameter, Type B active magnetic bearing has some advantages when compared with Type A: (a) the position and current constants k_p^b and k_i^b in (2) are two times bigger than their counterparts k_p^a and k_i^a in (1); (b) the cross section area A_b can be chosen greater than A_a; it is reasonable to have $A_b \approx 2A_a$; (c) the number of coils n_b can, possibly, be larger than n_a. The net conclusion is: the position (k_p) and current (k_i) constants for Type B AMBs have values at least 2 times higher than in case A. Depending on design aspects (A_b and n_b), even higher rates can be achieved. How much can these constants be increased? The magnetic saturation seems to be the limit.

To evaluate the effects of k_p and k_i in an AMB performance, a theorectical analysis was applied, in (David et al., 2014), to a control problem: a particle moving in a rectilinear path is to be positioned by magnetic devices that apply on it a force $f(t) = k_p x(t) + k_i i(t)$, where i is a control current and x is the displacement. A controller is desired, for driving x to 0 for all possible initial conditions, and in the eventual presence of constant, horizontal disturbance forces. This is a

simple, but meaningful, problem: many theorectical aspects of the real life operation and control of AMBs are present in it. PD and PID controllers were used, and the effects of k_p and k_i on the positioning problem an on the rejection of constant disturbances were analised. The conclusions, valid in much more general situations involving real world applications of practical interest, are that increasing the values of the magnetic force constants k_p and k_i is a highly desirable goal in the AMB field.

3. Prototype Building and Models

Theoretical considerations in (David et al., 2013) and (David et al., 2014) suggest that the interconnected fluxes in the type B structure increase the values of the magnetic force constants k_p and k_i. How sure can one be about the tools used in those developments? The idea of the Type B structure has already been tested in practice. In a prototype used at UFRJ (David, 2000), a vertical rotor is radially positioned by a self-bearing motor based on the interconnected fluxes of the type B structure. Such a situation is more complicated, because the windings are fed with AC currents, to achieve the dual capabilities of a self-bearing motor: torque generation and radial positioning. The device has worked!

The best possible way to answer these questions is by constructing and testing prototypes. Only after this stage, will the ideas proposed here be validated. Or not. Two prototypes, one for type A and the other for type B, have been constructed; figure 3 shows a top view of them. A vertical rotor with a large, perforated upper disk will fill the above pieces; the same Fig. 3, in the center, shows a view of a mounted kit, with the rotor inserted in the carcass with the stators.

Fig. 3 Top view of prototypes A, in the left and B in the right; notice the 8 “poles” in type A, and only 4 “poles” in type B. A mounted kit is shown in the center, with a vertical rotor inserted in one of the carcasses.

The vertical part details are depicted in the left side of Fig. 4. The bottom end is a mechanical bearing to prevent vertical movements; just above comes the rotor of a two-phase induction motor for spinning the shaft, and then the AMB rotor, the same for types A and B, and the sensors target. A disk with holes perforated near its edge lies on the upper part.

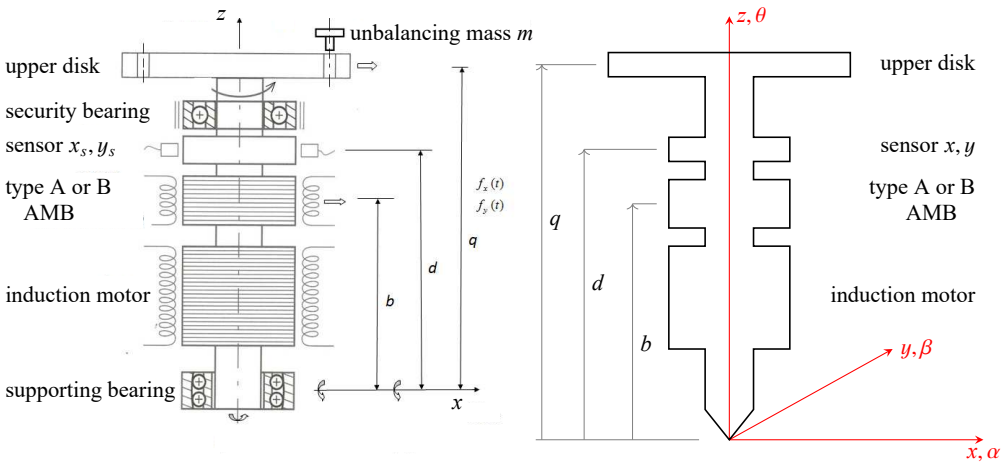

Fig. 4 Vertical rotor’s aspects and dimensions, in the left part. In the right half, a simplified representation of its basic geometric aspects and dimensions.

In order to find the mathematical model for the prototypes, the traditional procedures, (Schweitzer et al., 1994) (Chiba et al., 2005) (Schweitzer et al., 2009), will be used. The self aligning, supporting bearing at the bottom allows angular movements in any direction and provides a fixed point for the rotor. An inertial reference system is placed at this location; axes x and y lie in the horizontal plane and z marks the vertical direction. The positive angles α, β and θ can be found by using the right hand rule on x, y and z. The right half of figure 4 sketches the situation; the supporting and security bearings are not shown. Assuming a rigid and homogeneous rotor, the center of mass displacements can be determined by α and β, and a full dynamic model can be obtained from the rotational equations only. Denoting the angular moments of inertia around the three axes by I_x, I_y and I_z, symmetry considerations assure that $I_x = I_y = J$. The classical dynamic equations for rotations are

$$J\ddot{\beta}(t) - \omega I_z\dot{\alpha}(t) = E_\beta \qquad \text{and} \qquad J\ddot{\alpha}(t) + \omega I_z\dot{\beta}(t) = E_\alpha \tag{3}$$

where $\omega = \dot{\theta}$ is the rotor angular velocity and $E_{\beta,\alpha}$ express all external actions generating torques. The main equations above can be displayed in a vector form:

$$J\begin{bmatrix} \ddot{\beta} \\ -\ddot{\alpha} \end{bmatrix} + \begin{bmatrix} 0 & \omega I_z \\ -\omega I_z & 0 \end{bmatrix}\begin{bmatrix} \dot{\beta} \\ -\dot{\alpha} \end{bmatrix} = \begin{bmatrix} E_\beta \\ -E_\alpha \end{bmatrix}. \tag{4}$$

Defining the angular position vector $\boldsymbol{p} = [\beta \;\; -\alpha]^T$ and the external excitation vector $\boldsymbol{E} = [E_\beta \;\; -E_\alpha]^T$, the rotor dynamics is described by

$$J\ddot{\boldsymbol{p}}(t) + G\dot{\boldsymbol{p}}(t) = \boldsymbol{E}(t) \qquad \text{where} \qquad G = \begin{bmatrix} 0 & \omega I_z \\ -\omega I_z & 0 \end{bmatrix} = \omega I_z\begin{bmatrix} 0 & 1 \\ -1 & 0 \end{bmatrix} \tag{5}$$

is the gyroscopic matrix and J is the inertia coefficient (or the 2×2 inertia matrix $J\, I_2$). External torques may come from many different sources, four of which are consideredin this paper: $\boldsymbol{E} = \boldsymbol{E}_m + \boldsymbol{E}_g + \boldsymbol{E}_a + \boldsymbol{E}_d$.

Magnetic excitation $\boldsymbol{E}_m$: if x_b and y_b denote the rotor displacements at the AMB position, the forces generated in each direction are

$$f_x = k_p x_b + k_i i_x \qquad \text{and} \qquad f_y = k_p y_b + k_i i_y \tag{6}$$

where the differential currents i_x and i_y and the coefficients $k_{p,i}$ can be used with either type A or type B cases. Assuming rigidity and small angular displacements: $\beta \approx \sin\beta = x_b/b$ and $\alpha \approx \sin\alpha = -y_b/b$ which lead to $x_b \approx b\beta$ and $y_b \approx b(-\alpha)$. Equations (6) become $f_x = bk_p\beta + k_i i_x$ and $f_y = bk_p(-\alpha) + k_i i_y$. These forces cause torques $P_\beta = bf_x\cos\beta$ and $P_\alpha = -bf_y\cos\alpha$. Assuming, again, rigidity and small angular displacements: $\cos\beta \approx 1$ and $\cos\alpha \approx 1$ which lead to $P_\beta = bf_x$ and $P_\alpha = -bf_y$,that can be expanded as $P_\beta = b^2k_p\beta + bk_i i_x$ and $-P_\alpha = b^2k_p(-\alpha) + bk_i i_y$. If $\boldsymbol{E}_m = [P_\beta \;\; -P_\alpha]^T$ is the magnetical external excitation vector and $\boldsymbol{u} = [i_x \; i_y]^T$ is the external input or control vector, a concise expression is

$$\boldsymbol{E}_m = b^2k_p\boldsymbol{p} + bk_i\boldsymbol{u}. \tag{7}$$

Gravitational excitation $\boldsymbol{E}_g$: since α and β are small angles, the torques caused by the rotor weight are negligible: $\boldsymbol{E}_g \approx 0$. This is usually the case with vertical rotors; for horizontal ones, gravity must be considered.

Supporting bearing excitation $\boldsymbol{E}_a$: the bottom bearing has a viscous damper effect, generating torques modelled by $P_\beta = -C_a\dot{\beta}$ and $P_\alpha = -C_a\dot{\alpha}$ where C_a is a viscous constant. The external excitation contribution is

$$\boldsymbol{E}_a = \begin{bmatrix} P_\beta \\ -P_\alpha \end{bmatrix} = -C_a\begin{bmatrix} \dot{\beta} \\ -\dot{\alpha} \end{bmatrix} \quad \Longrightarrow \quad \boldsymbol{E}_a = -C_a\dot{\boldsymbol{p}} \tag{8}$$

Mass unbalancement excitation $\boldsymbol{E}_d$: rotors with an homogeneous mass distribution are assumed in the model preparation. When, and if, this is not true, unexpected forces and torques appear, acting as disturbances. If these actions are not considered in the control laws design, their effects can be unpleasant and even unnacceptable. The upper disk in the prototype rotor has 12 holes near the outer edge. They are placed in a symmetrical way, not to interfere with the body homogeneity, but extra masses can be placed in one of them to cause an intentional disturbance. A small mass m in one of the holes, as shown in figure 5, will act on the rotor with a centrifugal force $mr\dot{\theta}^2 = mr\omega^2$.

The projections of the centrifugal force on the x and y directions are $f_x^c = mr\omega^2\cos\theta$ and $f_y^c = mr\omega^2\sin\theta$. Since $\theta(t) = \omega t$, and considering the disk height q, the disturbance torques generated by the unbalanced mass are $P_\beta = mrq\omega^2\cos\omega t$ and $P_\alpha = mrq\omega^2\sin\omega t$. Therefore, the mass unbalancement external excitation contribution is

$$\boldsymbol{E}_d = \begin{bmatrix} P_\beta \\ -P_\alpha \end{bmatrix} = mrq\omega^2\begin{bmatrix} \cos\omega t \\ -\sin\omega t \end{bmatrix} = \Delta\boldsymbol{v}(t) \quad \text{where} \quad \Delta = mrq\omega^2 \quad \text{and} \quad \boldsymbol{v}(t) = \begin{bmatrix} \cos\omega t \\ -\sin\omega t \end{bmatrix} \tag{9}$$

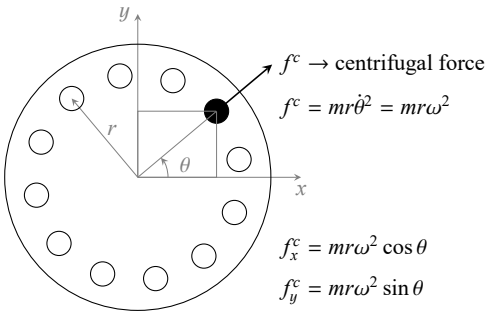

Fig. 5 Top view of the upper disk with an extra mass m filling one of the holes; the centrifugal force is projected on the x and y axes.

are, respectively, the disturbance coefficient and the disturbance input vector.

Entering the expressions obtained for the external excitations in equation (5) leads, after rearranging terms, to

$$J\ddot{\boldsymbol{p}}(t) + (G + C_a I_2)\,\dot{\boldsymbol{p}}(t) - b^2 k_p \boldsymbol{p}(t) = bk_i \boldsymbol{u}(t) + \Delta \boldsymbol{v}(t) \tag{10}$$

It is very convenient to rewrite this equation in terms of x_s and y_s, the positions measured by the sensors. Rotor rigidity, small angles and geometry considerations guarantee that$\beta \approx \sin\beta = x_s/d$ and $\alpha \approx \sin\alpha = -y_s/d$ which lead to $x_s = d\beta$ and $y_s = d(-\alpha)$. If the sensor measurements vector is denoted by $\boldsymbol{p}_s = [x_s\ y_s]^T$, then

$$\begin{bmatrix} x_s \\ y_s \end{bmatrix} = d \begin{bmatrix} \beta \\ -\alpha \end{bmatrix} \qquad \Longrightarrow \qquad \boldsymbol{p}_s = d\boldsymbol{p} \tag{11}$$

Multiplying (10) by d from the left, using (11) and dividing by J we reach the dynamic equation

$$\ddot{\boldsymbol{p}}_s + G_e \dot{\boldsymbol{p}}_s - K_e \boldsymbol{p}_s = B_2 \boldsymbol{u} + D_2 \boldsymbol{v} \ \text{ where } \ G_e = \frac{1}{J}(G + C_a I_2), \ \ K_e = \frac{b^2 k_p}{J}, \ \ B_2 = \frac{bdk_i}{J}, \ \ D_2 = \frac{mrqd\omega^2}{J} \tag{12}$$

in terms of the sensor positions. The state variables $\boldsymbol{x} = [\boldsymbol{p}_s^T\ \dot{\boldsymbol{p}}_s^T]^T = [x_s\ y_s\ \dot{x}_s\ \dot{y}_s]^T$ can be chosen, leading equation (12) to

$$\dot{\boldsymbol{x}}(t) = A\boldsymbol{x}(t) + B\boldsymbol{u}(t) + D\boldsymbol{v}(t) \tag{13}$$

where $\boldsymbol{x}$, $\boldsymbol{u}$ and $\boldsymbol{v}$ have been previously defined, A is a 4×4 matrix and B, D are 4×2 matrices structured as

$$A = \begin{bmatrix} 0 & I \\ A_{21} & A_{22} \end{bmatrix} \quad B = \begin{bmatrix} 0 \\ B_2 \end{bmatrix} \quad D = \begin{bmatrix} 0 \\ D_2 \end{bmatrix} \tag{14}$$

where the 2×2 blocks are

$$A_{21} = K_e I = \frac{b^2 k_p}{J} \begin{bmatrix} 1 & 0 \\ 0 & 1 \end{bmatrix} = A_{21}(k_p) \qquad \text{and} \qquad A_{22} = -G_e = \frac{-1}{J} \begin{bmatrix} C_a & \omega I_z \\ -\omega I_z & C_a \end{bmatrix} = A_{22}(\omega) \tag{15}$$

$$B_2 = \frac{bdk_i}{J} \begin{bmatrix} 1 & 0 \\ 0 & 1 \end{bmatrix} = B_2(k_i) \qquad \text{and} \qquad D_2 = \frac{mrqd\omega^2}{J} \begin{bmatrix} 1 & 0 \\ 0 & 1 \end{bmatrix} = D_2(m, \omega) \tag{16}$$

It is important to notice that equation (13) models a linear system that is time invariant only for a fixed rotational speed, because A_{22} depends on ω.

4. Prototype Simulations

The prototypes parameters were measured, in the SI system; the geometric dimensions are $b = 0.137, d = 0.203, q = 0.252, r = 0.060$; the inertia and viscous values are $m = 0.001, I_z = 0.0017, I_x = I_y = J = 0.0592, C_a = 0.0303$. A base current $i_0 = 3$ was used, leadind to $k_p^a = 207738, k_i^a = 27.70$ for type A and, for type B: $k_p^b = 830952, k_i^b = 110.79$. Assuming a constant $\omega = 100$rd/s (954rpm), the state space parameters A, B and D were calculated, generating matrices A_a, A_b etc. A state feedback control law $\boldsymbol{u} = F\boldsymbol{x}$ capable of stabilizing both models can be achieved with

$$F_a = \begin{bmatrix} -6073.8 & -25.5 & -3.5 & 0 \\ 25.5 & -6073.8 & 0 & -3.5 \end{bmatrix}.$$

The resulting closed-loop behaviour can be described by the eigenvalues of $A_a + B_a F = \{-22.2 \pm j113.8,\ -24.5 \pm j110.9\}$ and $A_b + B_b F = \{-90.1 \pm j211.5,\ -95.2 \pm j211.5\}$. Simulations, with F driving models $< A_a, B_a >$ and $< A_b, B_b >$ (calculated for a fixed $w = 100$rd/s) show that both cases are stabilized. Interesting results appear when an extra mass of 1g is fixed in the upper disk. There will be a mass unbalancement, and the harmonic forces at x and y will impose orbital movements to the rotor. The overall efficiency of the AMB control can be judged by the the radius of these orbits. A more complex simulation, with the model parameters now depending on ω (A_{21} and D_2 in (15) and (16)), was performed, for ω slowly varying from the rest condition to 250rd/s. The orbit radius for cases A and B is shown in figure 6.

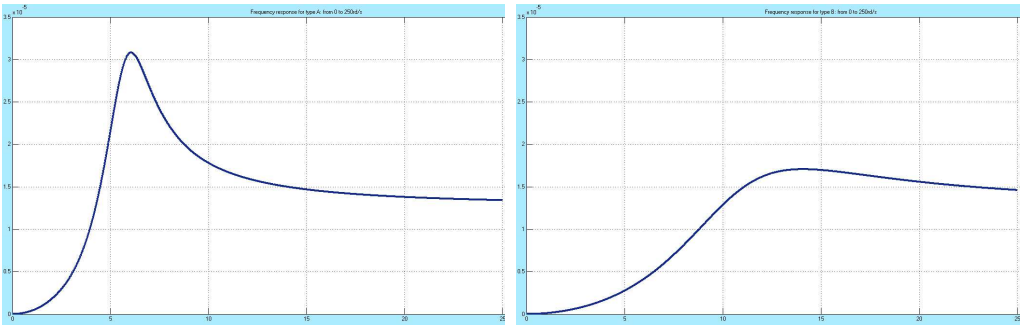

Fig. 6 Rotor orbital movements due to harmonic disturbances caused by a mass unbalancement in the upper disk; case A in the left and case B in the right. The high resonance in case A almost disappears in case B.

The sharp resonance in model A is almost completely eliminated, and shifted to a higher frequency, in case B. Other control laws $\boldsymbol{u} = F\boldsymbol{x}$ can be found that stabilize both models with a better dynamic behaviour that avoids resonances in their frequency response. In all these simulations, model B offers a clearly superior disturbance rejection characteristic. The bench tests to be made with the real prototypes will follow very closely the procedures used in these simulations.

5. Comments and Conclusions

The real prototypes are already finished and operational, but the laboratory tests are not in the final stages yet and no solid measurements has been made up to now. This means that sound statements can not be made yet. The authors have great expectations that the here called type B concept will be a valid contribution for the active magnetic bearings field, because of the possibility of increasing their equivalent mechanical stiffness.

References

Chiba A. and Fukao T. and Ichikawa O. and Oshima M. and Takemoto M. and Dorrell D., Magnetic Bearings and Bearingless Drives (2005), Newnes-Elsevier.

David D. F. B., Levitação de Rotor por Mancais-motores Radiais Magnéticos e Mancal Axial SC Auto-estável (2000), D.Sc. thesis in COPPE, Federal University of Rio de Janeiro, (in portuguese).

David D. F. B. and Santisteban J. A. and Del Nero Gomes A. C., Interconnected Four Poles Magnetic Bearings (2013), Proceedings of the 1st Brazilian Workshop on Magnetic Bearings, 2013, www.magneticbearings2103.com.br, october.

David D. F. B. and Santisteban J. A. and Del Nero Gomes A. C., Interconnected Four Poles Magnetic Bearings Simulations and Testing (2014), Proceedings of ISMB14, 14th International Symposium on Magnetic Bearings, 2014, pages 30–35, http://ismb14.magneticbearings.org, august.

Rodriguez E. F. and Santisteban J. A., An Improved Control System for a Split Winding Bearingless Induction Motor (2011), IEEE Transactions on Industrial Electronics, volume 58, number 8, pages 3401–3408.

Santos L. and Kjolhed K., Experimental Contribution to High-Precision Characterization of Magnetic Forces in Active Magnetic Bearings (2007), Journal of Engineering for Gas Turbines and Power, volume 129, pages 503– .

Schweitzer, G. and Bleuler, H. and Traxler, A., Active Magnetic Bearings (1994), Hochshulverlag AG an der ETH Zürich.

Schweitzer, G. and Maslen E. and Bleuler, H. and Cole M. and Keogh P., Magnetic Bearings: Theory, Design and Applications to Rotating Machinery (2009), Springer-Verlag.